Journal of Electronic Materials (2024) 53:5169–5183
https://doi.org/10.1007/s11664-024-11178-7

28TH INTERNATIONAL CONFERENCE ON NUCLEAR TRACKS AND RADIATION MEASUREMENTS

Structural, Ferroelectric, and Ferromagnetic Properties of Yttrium-Doped Cobalt Ferrites to Produce Green Electricity by Hydroelectric Cells

Prachi Jain[1,2] · S. Shankar[2] · O. P. Thakur[1]

Received: 29 January 2024 / Accepted: 10 May 2024 / Published online: 11 June 2024

Abstract

A hydroelectric cell has been coined as an accomplished device keeping the ability to produce current just by adsorbing a few microliters of water. These cells are the new source of generating green energy which involves no evolution of toxic gases like NO_2, SO_2, CO, etc. Our current research focuses on studying how to increase the maximum output current (I) in the pure cobalt ferrites by doping with rare-earth ion, yttrium. The yttrium-doped cobalt ferrites with composition ($CoY_xFe_{2-x}O_4$, $x = 0.00$, 0.10, and 0.20) have been prepared using a modified sol–gel citrate method. X-ray diffractogram (XRD) confirmed the formation of cubic crystal structures with crystallite size less than 30 nm. Energy dispersive x-ray (EDX) patterns confirmed the presence of elements (Y, Co, Fe, O) in the prepared compositions. The ionic diffusion mechanism confirmed the dissociation of water molecules by the cations present on the surface of the material at room temperature. Vibrating sample magnetometer (VSM) analysis revealed the increase in coercivity values from 948.81 Oe to 2580.09 Oe with the increase in the concentration of yttrium ions in the cobalt ferrite (CFO) lattice. The V–I polarization curves measured the maximum output current and voltage as around 8.6 mA and 1.1 V, respectively, for the 20% yttrium-doped CFO hydroelectric cells (area = 4 cm^2).

Keywords Multiferroics · spinel ferrites · hydroelectric cells · ionic diffusion · ferroelectrics

Introduction

Ferrites have now become a current era of research due to their coverage of useful applications in many fields, like biomedical, environmental engineering, material chemistry, mechanical studies, etc.[1] A variety of ferrites have been utilized with 2D materials to make electrodes in supercapacitors to provide more stability to the material. Ferrites are broadly classified into 3 main types: spinel, garnet, and hexa-ferrites. Here, we will study the structure, morphology, and properties of spinel ferrites which are capable of producing stable hydroelectric cells. The hydroelectric cell is a device that is based on the mechanism of the conversion of water into electrical energy.[2] Cobalt ferrites are in the category of hard ferrites, which are highly coercive and highly magnetic with good chemical stability. The cobalt ferrite has an inverse spinel close-packed cubic structure where O^{2-} ions occupy all 8 corners of the cubic lattice, and Co^{2+}, and Fe^{3+} ions occupy both tetrahedral and octahedral sites.[3] Since cobalt ferrites keep half the value of magnetization as compared to ferromagnetic alloys, have a few advantages like heat resistance, high coercivity, low eddy current losses, high corrosion resistance, and low prices. It is well known that doping with rare-earth elements in spinel ferrites can drastically change their magnetic properties. For example, doping with Gd^{3+}, Eu^{3+}, and Nd^{3+} causes a reduction in magnetic saturation (M_s), while other properties like

✉ S. Shankar
shankar3274@gmail.com; sssubramaniam@arsd.du.ac.in

✉ O. P. Thakur
opthakur@nsut.ac.in

[1] Materials Analysis and Research Laboratory, Department of Physics, Netaji Subhas University of Technology, New Delhi 110078, India

[2] Functional Materials Research Laboratory, Department of Physics, ARSD College, University of Delhi, New Delhi 110021, India

coercivity (H_c) and magneto-crystalline anisotropy (K_1) are increased.[4–6] Additionally, it has been found that doping of yttrium, (Y^{3+}) ions in cobalt ferrites causes a reduction in the M_s with an increment in the H_c values when prepared by the citrate method.[7] Doping of rare-earth ions can enhance the electrical and magnetic properties of cobalt ferrites. However, the enhancement depends upon the synthesis procedure, the crystallite size of nanoparticles, heat treatment, and other factors, which are also involved in deciding the electrical properties of spinel ferrites.[8] Recently, the generation of electric currents through hydroelectric cells has made its first breakthrough invention which generates energy by dissociating water molecules using lithium-doped magnesium ferrites ($Mg_{0.8}Li_{0.2}Fe_2O_4$).[9] Magnesium cations have a high affinity to pair with OH^- ions, whereas oxygen vacancies dissociate the polar water molecules into H_3O^+ and OH^- ions.[10] The ions that have been dissociated were collected at Ag and Zn electrodes. Hydroelectric cells have also been fabricated using other metal oxides like ZnO, SnO_2, MgO, TiO_2, etc.[11] Maximum offload power was delivered around 27 mW for hydroelectric cells fabricated using hematite.[12] Even though there are many spinel ferrites on which hydroelectric cell studies have been carried out, studies of hydroelectric cell applications based on rare-earth-doped spinel ferrites are very limited. Therefore, in the present work, we have carried out an investigation on the structural, magnetic, and hydroelectric cell properties of yttrium-doped cobalt ferrites ($CoY_xFe_{2-x}O_4$, $x = 0.00$, 0.10 and 0.20). The values of maximum current, voltage, and power are reported on fabricated hydroelectric cells of yttrium-doped cobalt ferrites. Due to the mismatch in the ionic radii of Y^{3+} and Fe^{3+} ions, a small value of the microstrain is induced. This induced strain will then produce defects in the lattice of the spinel ferrites.[13] These oxygen defects play a vital role in chemi-dissociating the water molecules on the sample surface.

Compared to the recent literature reported on CoYFeO4 systems, no work has been reported on the fabrication of hydroelectric cells, which are the cells that are meant to produce a current without any use of an external electrolyte. It has been observed that, for $x = 0.10$, the value of magnetization was found to be around 49.03 emu/g, which is higher than the value reported for the same doping of yttrium in CFO ($M_s = 28.08$ emu/g).[14] Ferroelectric polarization loops have also been shown in the prepared material, and higher than in the latest literature, and not reported in the proposed literature.[15] The present work demonstrates the enhancement in the current values of cobalt ferrite-based hydroelectric cells (HECs) upon substitution of rare-earth (yttrium) ions. The novelty of this work is making the comparison with all recent reported literature focusing on spinel ferrites. It has been revealed that, for the given HEC cell area of 4 cm^2, a maximum current of 8.6 mA has not yet been reported for yttrium-substituted cobalt ferrites which proves the novelty of our work. A critical comparison between the results and similar system(s) for the same application are discussed in Table VIII (below).

Synthesis Procedure

The precursors, cobalt nitrate ($Co(NO_3)_2{\cdot}6H_2O$; Sigma Aldrich, 99% purity), ferric nitrate nonahydrate ($Fe(NO_3)_3{\cdot}9H_2O$; Loba Chemie, 98% purity) and yttrium nitrate hexahydrate ($Y(NO_3)_3{\cdot}6H_2O$; Sigma Aldrich, 99.9% purity) were measured as per their calculated weight and were allowed to dissolve in DI water at 300 rpm for 30 min each. Meanwhile, a 1 M solution of citric acid was prepared and kept on a magnetic stirrer for 30 min. Then, all the as-prepared separate solutions were added in the citric acid solution. Citric acid ($C_6H_8O_7$) works as a chelating agent to avoid the aggregation of the nanoparticles formed as it keeps the tendency to become adsorbed on the metal oxide surfaces. Due to its easier adsorption on the ferrite's surface, this makes the surface of the nanoparticles hydrophilic and helps in the homogenous dissolution of metal ferrites with each other.[16] After that, the pH of the solution was balanced to 8–9 until the solution became black in color. It has been noticed that the value of pH more than 10 indicates larger-sized nanoparticles. So, the value of pH was adjusted between 8 and 9 to obtain smaller-sized nanoparticles along with improved magnetization compared with those whose pH lies between 7 and 8.[17] After that, the solution was kept on heating at 80 °C to form a dark black powder which was then ground in an agar pestle and mortar for 1 h and sintered at 800 °C for 4 h with a heating rate of 5 °C/min. The step-by-step detailed synthesis procedure is shown in Fig. S1 (see online supplemental material). The amount of precursors taken for synthesizing each compound is shown in Table I.

Table I Amount of precursors taken in synthesizing each composition of yttrium-doped cobalt ferrites using sol–gel auto-combustion synthesis

Composition ($CoY_xFe_{2-x}O_4$)	Precursors			
	$Co(NO_3)_2{\cdot}6H_2O$	$Fe(NO_3)_3{\cdot}9H_2O$	$Y(NO_3)_3{\cdot}6H_2O$	Citric acid
$X = 0.00$	2.64	7.35	–	15.23
$X = 0.10$	2.36	7.29	0.345	15.60
$X = 0.20$	2.08	7.23	0.685	15.42

Fabrication of Hydroelectric Cells (HECs)

The complete procedure for the preparation of yttrium-doped cobalt ferrite HECs is shown in Fig. S2. The obtained sample powder was transformed into square pellets of area 4 cm^2 using a hydraulic presser with pressure 15 KPa under 2-min holding time. The pellets were then densified by sintering at 500 °C for 2 h to evaporate the polyvinyl alcohol. After that, the silver electrodes in a comb-shaped pattern were drawn on one side of the pellet and the other side was pasted onto a zinc sheet. Finally, 0-mm electrical wires were soldered on both sides of the pellets to measure the *V–I* response of the cell.

Characterization

Polycrystalline powder of yttrium-doped cobalt ferrites ($CoY_xFe_{2-x}O_4$, $x = 0$, 0.10 and 0.20) was prepared using a sol–gel auto-combustion route and was utilized for several structural measurements. The prepared samples were first characterized by x-ray diffraction (XRD; Rigaku) with Cu-Kα radiation having the wavelength ($\lambda = 1.5406$ Å) to analyze the structural formation and shape of the unit cell. Fourier-transform infrared (FT-IR; iS50; Nicolet) analysis measurements were taken to check the compositional characteristics in the sample. The surface morphology of the samples was taken using field-emission scanning electron microscopy–energy dispersive x-ray (FESEM-EDX; Zeiss) measurements. A vibrating-sample magnetometry (VSM) study was carried out to measure the highest value of magnetic saturation in the samples. *V–I* measurements were carried out using a Keithley 2450 source meter to check the maximum output current and voltage produced in the fabricated HECs.

Results and Discussion

XRD Morphology

The XRD patterns of the yttrium-doped cobalt ferrite nanoparticles ($CoY_xFe_{2-x}O_4$, $x = 0.00$, 0.10, and 0.20) were carried out at room temperature (RT), as shown in Fig. 1. The indexing of all the peaks has been carried out using the JCPDS card number #22-1086.[18] The XRD pattern confirms the formation of inverse cubic spinel structure with space group Fd-3m. One impurity peak at $2\theta = 33.1°$ corresponds to the formation of the Fe_2O_3 hematite phase.[19] This peak is inherent and occurred due to the addition of ethylene glycol during the synthesis of the spinel ferrites.[16] The impurity % of Fe_2O_3 was found to be less than 1% and this peak is generally formed due to the hematite phase.

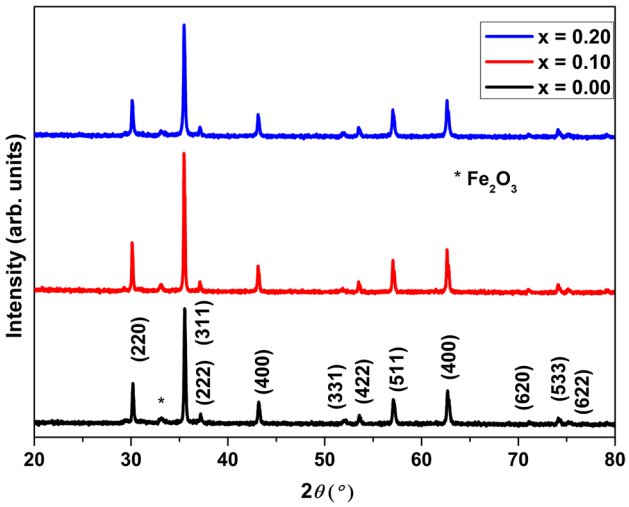

Fig. 1 XRD patterns of the yttrium-doped cobalt ferrites ($CoY_xFe_{2-x}O_4$, $x = 0.00$, 0.10, 0.20) obtained at room temperature.

The values of all the useful parameters like lattice parameters, crystallite size, x-ray density, bulk density, and porosity are set out in Table II and given by:

$$\text{Lattice parameter } (a) = d\sqrt{h^2 + k^2 + l^2} \quad (1)$$

where a is the lattice parameter, d is the interplanar spacing, and (h k l) are the crystal planes occurring at particular peak positions.

$$\text{Crystallite size } (D) = k\lambda/\beta \text{Cos}\theta \quad (2)$$

where θ denotes the peak positions, β represents the full width half-maxima, and D is the crystallite size calculated using the Debye–Scherrer equation, $K = 0.9$, and $\lambda = 1.5406$ Å.

$$\text{X - ray density } \left(D_x\right) = \frac{8M}{Na^3} \quad (3)$$

where D_x is the x-ray density, M is the molecular weight, and N is Avogadro's number.

$$\text{Bulk density } \left(D_b\right) = \text{Mass of pellet } (m)/\text{Volume of pellet } (\pi r^2 l) \quad (4)$$

where D_b is the bulk density, r is the radius of the prepared pellet, l is the height of the pellet, and $\pi = 3.14$.

$$\text{Porosity } (\%) = 1 - D_b/D_x \quad (5)$$

It has been observed that the lattice parameter (a) has been increased from 8.37 Å to 8.39 Å with the increase in doping % of yttrium from 0% to 20%. This rise in the lattice constant occurs due to the difference in ionic radii of Fe^{3+} (0.65 Å) and Y^{3+} ions (0.95 Å). Additionally, it has been observed that the bulk as well as the x-ray densities are also increasing on adding

yttrium ions. This is mainly due to the difference in molar masses of yttrium (88.9 g/mol) and iron (55.84 g/mol) atoms.[20]

Williamson–Hall (*W–H*) plots have been plotted for yttrium-doped cobalt ferrites, as shown in Fig. 2a, b, and c. The values of crystallite size and strain have been calculated using the *W–H* plot equation given by[21:]

$$\beta_{hkl} Cos\theta = \varepsilon(4Sin\theta) + \frac{K\lambda}{D} \quad (6)$$

where ε is the micro-strain, θ is Bragg's angle, and $K\lambda$ is a constant value equal to 1.38654.

The doping of Y^{3+} ions in cobalt ferrite caused contraction or expansion in the cobalt ferrite lattice which induces the micro-strain. As a result, oxygen defects have been created due to the different valencies of the (Co^{2+}, Y^{3+}, Fe^{3+}/Fe^{2+}) ions and the difference in their ionic radii. The three-dimensional cubic structures of pure as well as yttrium-doped cobalt ferrites are shown in Fig. 3 obtained using VESTA software. Since the doping of Y^{3+} ions helped in creating more oxygen defects along with the rise in porosity value, more defective structures would be able to dissociate more water molecules. Thus, the yttrium ions have been

Table II Values of crystallite size, strain, volume, and density for yttrium-doped cobalt ferrites ($CoY_xFe_{2-x}O_4$) prepared using sol–gel auto-combustion

Composition	Crystallite size (nm)	Strain	Lattice parameter ($a = b = c$) (Å)	Volume (Å^3)	Porosity	Bulk density (g/cm^3)	X-ray density (g/cm^3)
$X = 0.00$	36.83	0.00118	8.37	587.83	0.57	2.26	5.26
$X = 0.10$	32.48	0.00157	8.38	590.17	0.58	2.26	5.31
$X = 0.20$	25.87	0.00246	8.39	591.35	0.59	2.26	5.61

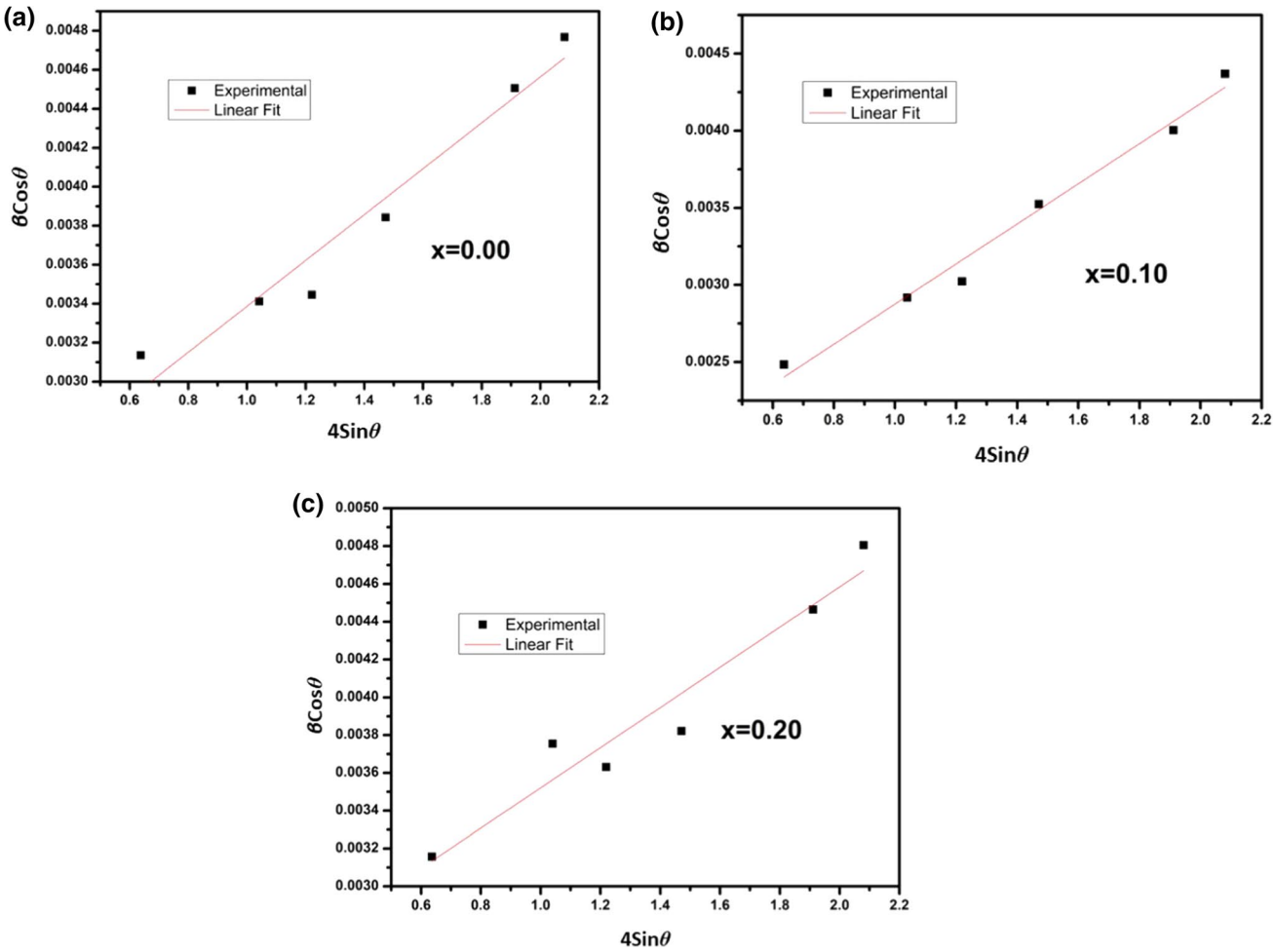

Fig. 2 Williamson–Hall (*W–H*) plots of the yttrium-doped cobalt ferrites ($CoY_xFe_{2-x}O_4$), (a) $x = 0.00$, (b) $x = 0.10$, and (c) $x = 0.20$).

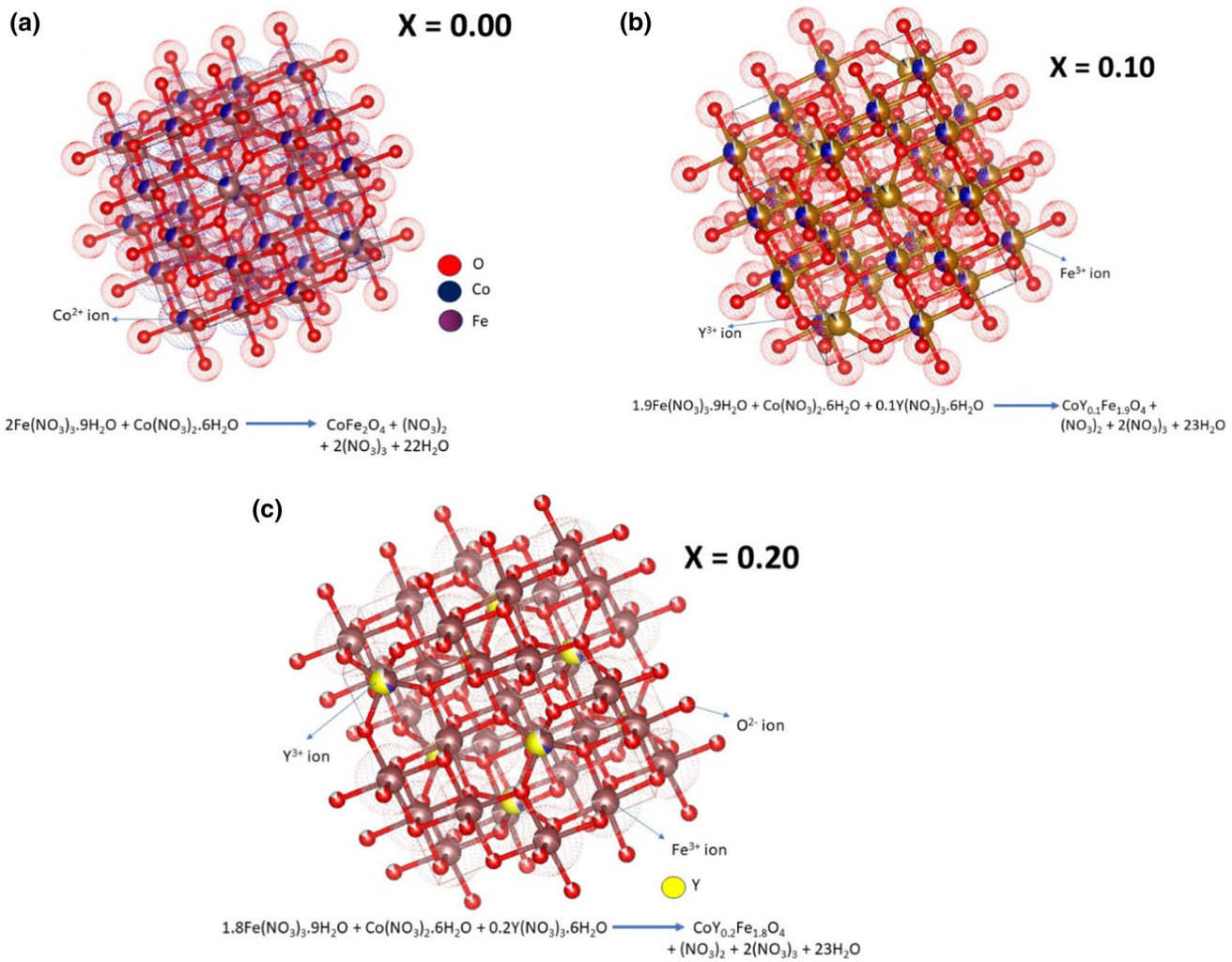

Fig. 3 3-D structure of yttrium-substituted cobalt ferrites ($CoY_xFe_{2-x}O_4$), (a) $x = 0.00$, (b) $x = 0.10$, and (c) $x = 0.20$.

proven to be useful dopants in improving the water dissociation efficiency of pure cobalt ferrites.

Rietveld Refinement

All the peaks obtained in the XRD patterns have been refined using Rietveld refinement, as shown in Fig. 4a, b, and c. The whole refinement process has been performed using FULLPROF software. With the help of this refinement, the other useful parameters like cation distribution, the volume of the unit cell, the density of the lattice, lattice parameters, interplanar spacing, etc. can be readily calculated. The refinement has been carried out by assuming the profile as Thompson–Cox pseudo-Voight. The refinement was carried out by refining the global parameters such as background and scale factors, shape parameters, background correction, metal ion occupancies, atomic coordinates, and isothermal parameters. It has been observed that Y^{3+} ions are replacing the iron ions from their tetrahedral lattice sites.[15] The difference in their valencies is the main reason behind the production of oxygen vacancies, which would automatically account for more water adsorption. The distribution of cations over the A and B lattice sites is shown in Table III.

FESEM Morphology

FESEM-EDX spectra for pure as well as yttrium-doped cobalt ferrite nanoparticles are shown in Fig. 5a, b, and c. The FESEM images show the irregularly shaped nanoparticles with slight agglomerations present at the corners. EDX analysis confirms the presence of elements Co, Y, Fe, and O in the yttrium-doped cobalt ferrite samples. The variation of grain size and standard deviation with the rise in the doping % of yttrium ions in cobalt ferrites are listed in Table IV. The atomic % for all the atoms present in each composition are set out in Table V. It has been found that the average particle size varies from 80.96 nm to 49.09 nm with increasing Y^{3+} concentration in the cobalt ferrites. The particle size distribution histograms

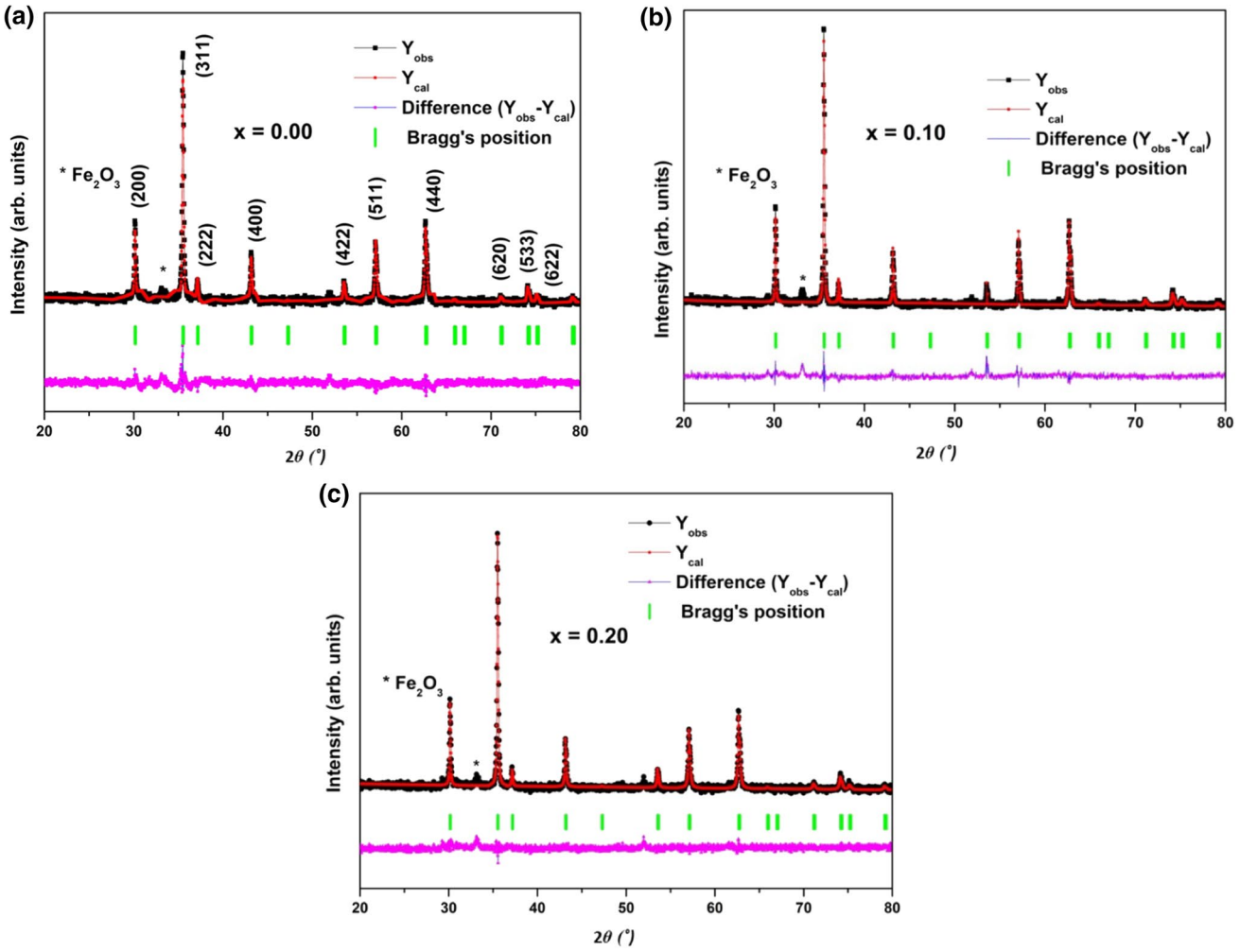

Fig. 4 Rietveld-refined XRD patterns for yttrium-doped cobalt ferrites ($CoY_xFe_{2-x}O_4$), (a) $x = 0.00$, (b) $x = 0.10$, and (c) $x = 0.20$).

Table III Distribution of cations obtained through Rietveld refinement using FULLPROF software

Sample no.	Sample name ($CoY_xFe_{2-x}O_4$)	A-site (Tetrahedral)	B-site (Octahedral)
1.	$X = 0.00$	$(Co_{0.2}{}^{2+}Fe_{0.8}{}^{3+})_A$	$(Co_{0.8}{}^{2+}Fe_{1.2}{}^{2+})_A$
2.	$X = 0.10$	$(Co_{0.09}{}^{2+}Y_{0.10}Fe_{0.81}{}^{3+})_A$	$(Co_{0.91}{}^{2+}Fe_{1.09}{}^{2+})_A$
3.	$X = 0.20$	$(Co_{0.08}{}^{2+}Y_{0.20}Fe_{0.72}{}^{3+})_A$	$(Co_{0.92}{}^{2+}Fe_{1.08}{}^{2+})_A$

for all the compositions have been separately plotted, as shown in Fig. 6a, b, and c. The log-normal distribution function has been used for fitting histograms and estimating the average particle size values for the different compositions of yttrium-doped cobalt ferrites. The log-normal function[22] is given by:

$$f(D) = \frac{1}{\sqrt{2}\pi\sigma_D} \exp \frac{-\ln \frac{D}{D_o}}{2\sigma^2} \quad (7)$$

where D is the average particle size and σ_D is the mean standard deviation.

Magnetic Studies

Magnetic measurements of the yttrium-doped cobalt ferrites ($CoY_xFe_{2-x}O_4$, $x = 0.00, 0.10, 0.20$) have been performed at RT under the magnetic fields varying from − 1 T to + 1 T, as shown in Fig. 7a. The increased value of coercivity (H_c) in all the samples indicates that the prepared samples are hard magnets or hard ferrites at RT. The *M–H* curves are strongly

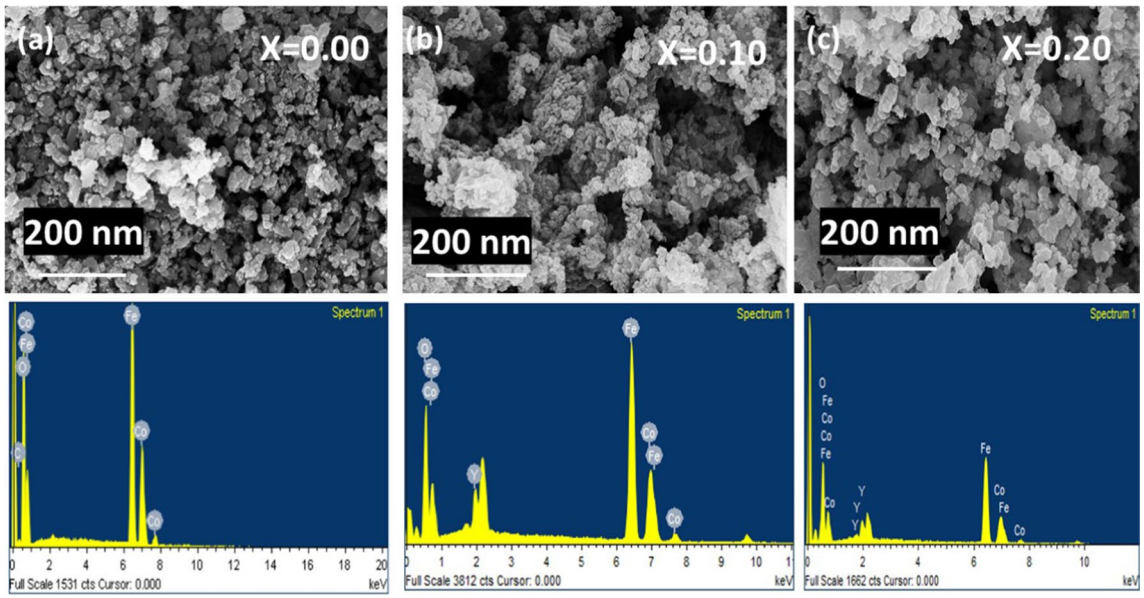

Fig. 5 FESEM-EDX micrographs of the yttrium-doped cobalt ferrites ($CoY_xFe_{2-x}O_4$), (a) $x = 0.00$, (b) $x = 0.10$, and (c) $x = 0.20$.

Table IV Values of grain sizes and standard deviations of the prepared samples

Composition	Grain size (nm)	Standard deviation
$X = 0.00$	80.96	8.54
$X = 0.10$	59.85	7.54
$X = 0.20$	49.09	4.52

Table V Atomic % of all elements present in a prepared composition of yttrium-doped cobalt ferrites

Different doping % of yttrium ions in cobalt ferrite	Atomic %			
	Co	Fe	O	Y
0%	16.33	34.74	48.93	–
10%	15.13	35.78	45.71	3.38
20%	10.87	38.90	43.78	6.45

dependent upon the doping of Y^{3+} ions. It has been noticed that the value of saturation magnetization (M_s) decreases from 54.23 emu/g to 36.84 emu/g, and that the coercivity values have increased from 968.76 Oe to 2598.18 Oe on doping with Y^{3+} ions in cobalt ferrite. On the other hand, values of H_c for yttrium-doped cobalt ferrites are found to be larger than cobalt ferrites doped with Nd^{3+}, Gd^{3+}, and Eu^{3+} ions.[23,24] The values of coercivity depend on various factors such as particle size, micro-strain, magnetic domain size, etc. For the particles exhibiting a multi-domain nature, the coercivity varies inversely proportional to the particle size.[20] Here, the particle size is decreasing by increasing the Y^{3+} ion concentration, as depicted from the FESEM morphology. As a result, the coercivity values increase upon the rise in Y^{3+} ion doping. Thus, doping of Y^{3+} ions is preferable in CFO to achieve a high value of coercivity at RT. Table VI includes the values of all the useful magnetic parameters (M_s, H_c, M_r, squareness ratio) obtained through the VSM study. It has also been reported by Chakrabarty et al. [25] that the reduction in magnetization with rising yttrium content in cobalt ferrites mainly depends on two factors. First, the magnetic exchange interactions of ions at the A–A, B–B, and A–B lattice sites, and, second, due to the smaller involvement of Y^{3+} with the nearest ions due to its zero magnetic moment. The reduction of M_s with yttrium-doping is basically due to the zero magnetic moment of yttrium ions substituting iron ions with a very high magnetic moment. Since yttrium is a non-magnetic ion, substituting a magnetic ion (Fe^{3+}) from its octahedra position to a tetrahedra position would lead to a reduction in the magnetization values on B-sites. As a result, the net saturation magnetization decreases and the coercivity increases. Figure 9b shows the enlarged *M–H* plot exhibiting the increase in the coercive nature of cobalt ferrites with the rise in yttrium-doping. The increment in the coercivity (H_c) to 2598 Oe makes yttrium-doped cobalt ferrites a suitable candidate for fabricating hard-core magnets which are very difficult to demagnetize. The saturated magnetization is always considered at low temperatures because the quantum confinement effect becomes more dominating, which means the arrangement of spins of electrons on the surface and alignment of domains towards the applied field. Generally, ferrites make the phase transition at a specific value

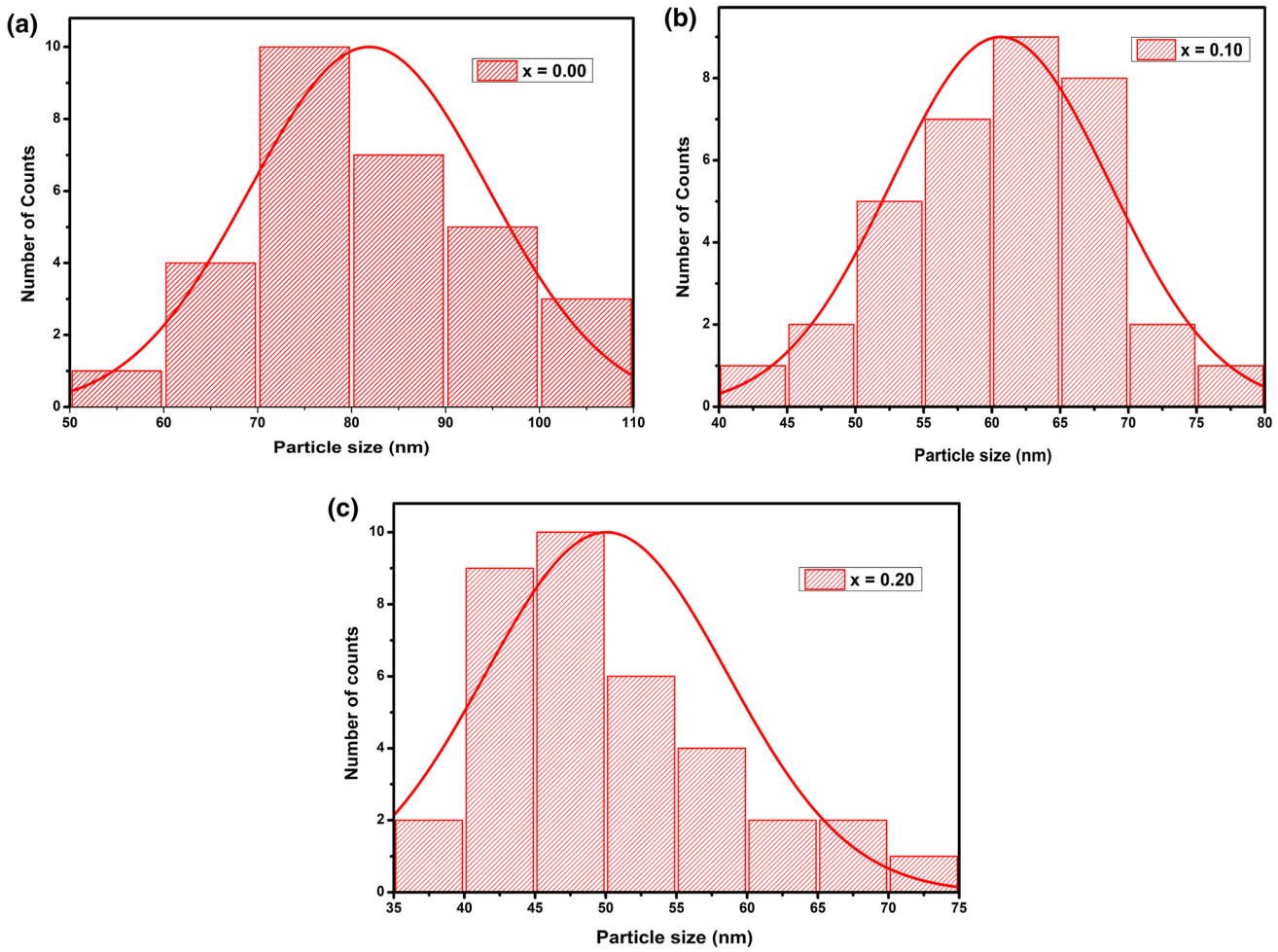

Fig. 6 Size distribution histograms obtained for the yttrium-doped cobalt ferrites ($CoY_xFe_{2-x}O_4$), (a) $x = 0.00$, (b) 0.10, and (c) $x = 0.20$ obtained using ImageJ software.

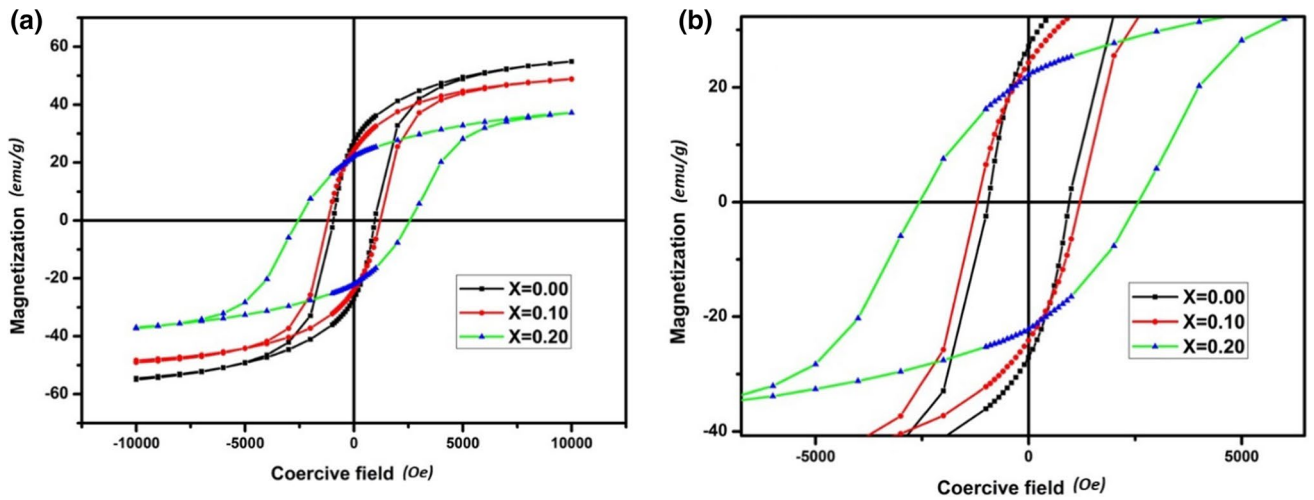

Fig. 7 (a) Plot of magnetization against coercive field for yttrium-doped cobalt ferrites obtained at room temperature, (b) M_s and H_c versus concentration of yttrium ions.

Table VI Magnetic parameters of $CoY_xFe_{2-x}O_4$ nanoparticles with $x = 0.0$, 0.10 and 0.20 at room temperature

Composition	Magnetic parameters				
	M_s (emu g^{-1})	H_c (Oe)	M_r (emu g^{-1})	Squareness ratio (M_r/M_s)	Nature
$X = 0.00$	54.66	948.81	27.19	0.497	Single-domain
$X = 0.10$	49.03	1190.48	24.16	0.492	Single-domain
$X = 0.20$	36.76	2580.09	22.23	0.604	Multi-domain

of temperature which can be called the Curie temperature. So, studying the magnetic properties at low-temperature values will automatically help in studying the behavior at the Curie temperature. Most of the ferrites exhibit stable magnetic properties at RT which would thereby be helpful in yielding reliable and consistent readings. The measurements taken at RT also make the comparison of the already reported data easier. In the present study, the focus is only on the RT magnetic properties of doped spinel ferrites. It is quite evident that the crystallite size has been decreasing with increasing doping % of Y^{3+} ions in the cobalt ferrites. The decrease in the crystallite size with the rise in yttrium ions might be another reason behind the reduction in magnetization because it increases the dis-orderness in the spin magnetic moments. This behavior has caused a reduction in magnetization due to increased lattice distortion because the surface effect becomes more pronounced with the reduction in the crystallite size.[26] Due to the effect of lattice strain on the surface atoms, vacancies in the lattice will occur, which results in distortion, varying interplanar spacings, and interatomic spacings. All these factors gave rise to disordered spin states and hence reveal reduced saturation magnetization.

Squareness Ratio

The existence of different types of exchange groups present within the grains is determined by the ratio of M_r/M_s, known as the squareness ratio (SQR). As per the previous literature, if the SQR is less than 0.5, then the sample contains single-domain superparamagnetic nanoparticles.[27] If this ratio > 0.5 and less than 1, then the prepared samples conceive a multi-domain ferromagnetic nature. Also, according to Stoner's theory, the anisotropy is defined on the basis of SQR. If SQR < 0.5, then uniaxial anisotropy is formed, but if SQR > 0.5, then cubic anisotropy is formed. Here, after doping of 10% or for 20% Y doping, the SQR becomes greater than 0.5, which means that cubic anisotropy is formed upon 20% doping of Y^{3+} ions in cobalt ferrites.

Ferroelectric Studies

The variation of polarization with respect to the electric field for the different compositions of yttrium-substituted cobalt ferrites is shown in Fig. 8. All the *P–E* measurements have

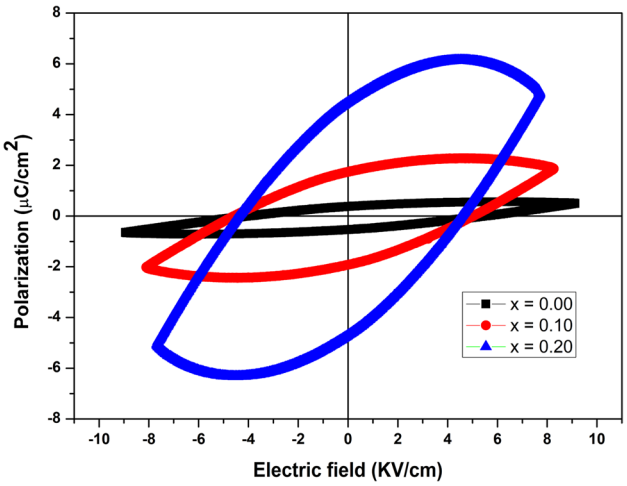

Fig. 8 Ferroelectricity in yttrium-doped cobalt ferrites ($CoY_xFe_{2-x}O_4$, $x = 0.00$, 0.10, and 0.20) obtained at room temperature.

been carried out under an electric field of 6 KV/cm. The obtained *P–E* loops exhibit a weak ferroelectric nature due to high leakage currents occurring in the spinel ferrites. The high leakage current is mainly due to the presence of a high number of oxygen vacancies.[28] The behavior of the obtained *P–E* loops is of lossy conductor type. Pure cobalt ferrites conceive a minimum area and hence consist of lossy capacitor-type behavior. It has been observed that the net saturation ferroelectric polarization value has been increased to 6.377 μC/cm^2 for $x = 0.20$. The doping of yttrium ions caused the structural deformation in the structure of the cobalt ferrites, which has occurred due to the difference in the ionic radii of Fe and Y ions.[29] The distortion in the structure caused the overall improvement in the ferroelectric nature of the yttrium-doped cobalt ferrites. Electric coercivity is a measure of the electric field strength which is required to reverse the polarization of a dielectric material. Increased coercivity suggests the strength of material needed to retain its dielectric behavior. In our material, the reduced electric coercivity suggests the production of more free charge carriers with the applied external electric field. With the increase in the doping % Y^{3+} ions, the amount of free charge carriers produced increased, due to which its net electric coercivity decreased. The release of more free charge carriers will facilitate more

conduction, which would be helpful in producing more value of currents in HECs.

V–I Polarization Curves

The variation of current and power against voltage for the yttrium-doped cobalt ferrite-based HECs is shown in Fig. 9a, b, and c. The maximum offload current around 8.6 mA and maximum voltage nearly equal to 1.13 V have been achieved for 20% yttrium-doped cobalt ferrites HECs. The current value for pure cobalt ferrite HECs of area 4 cm^2 is measured to be around 6.2 mA. The jump in current value from 6.2 mA to 8.6 mA is mainly due to more water adsorption by the oxygen vacancies present on the surface of the doped cobalt ferrite HECs. Doping of Y^{3+} ions caused contraction/expansion of the cobalt ferrite lattice due to which small value of strain is induced. This induced strain creates some defects in the lattice and, as a result, the water molecules are adsorbed by these defects leading to the small value of the current.[30]

All the HEC parameters for all the prepared compositions are set out in Table VII. The *V–I* polarization curve is categorized into three parts, named as: activation loss (PQ), ohmic loss (QS), and concentration loss (RS). PQ generally provides the potential needed to overcome the reaction taking place on the surface of the HEC. The QS signifies the ohmic loss which is mainly due to the resistance offered by the substitution of cobalt ions by the yttrium ions. RS represents the mass concentration loss, which generally occurs due to the coagulation of ions on the surface electrode.[31,32] The mass concentration loss is a minimum for 10% yttrium-doped CFO-based HECs. Thus, 10% Y doping is meant to be the most preferable among the three compositions. A comparative study on the spinel ferrite-based HECs have been carried out as shown in Table VIII.

Working Mechanism of the Hydroelectric Cells

The splitting of water molecules on the ferrite surface is initiated when water molecules make contact with the surface

Table VII Hydroelectric cell parameters calibrated through *V–I* curves

Composition	Current (mA)	Voltage	Power	Activation loss	Concentration loss
$X = 0.00$	6.2	1.00	6.30	0.36	0.35
$X = 0.10$	8.2	0.76	6.35	0.22	0.004
$X = 0.20$	8.6	1.13	9.85	0.47	0.18

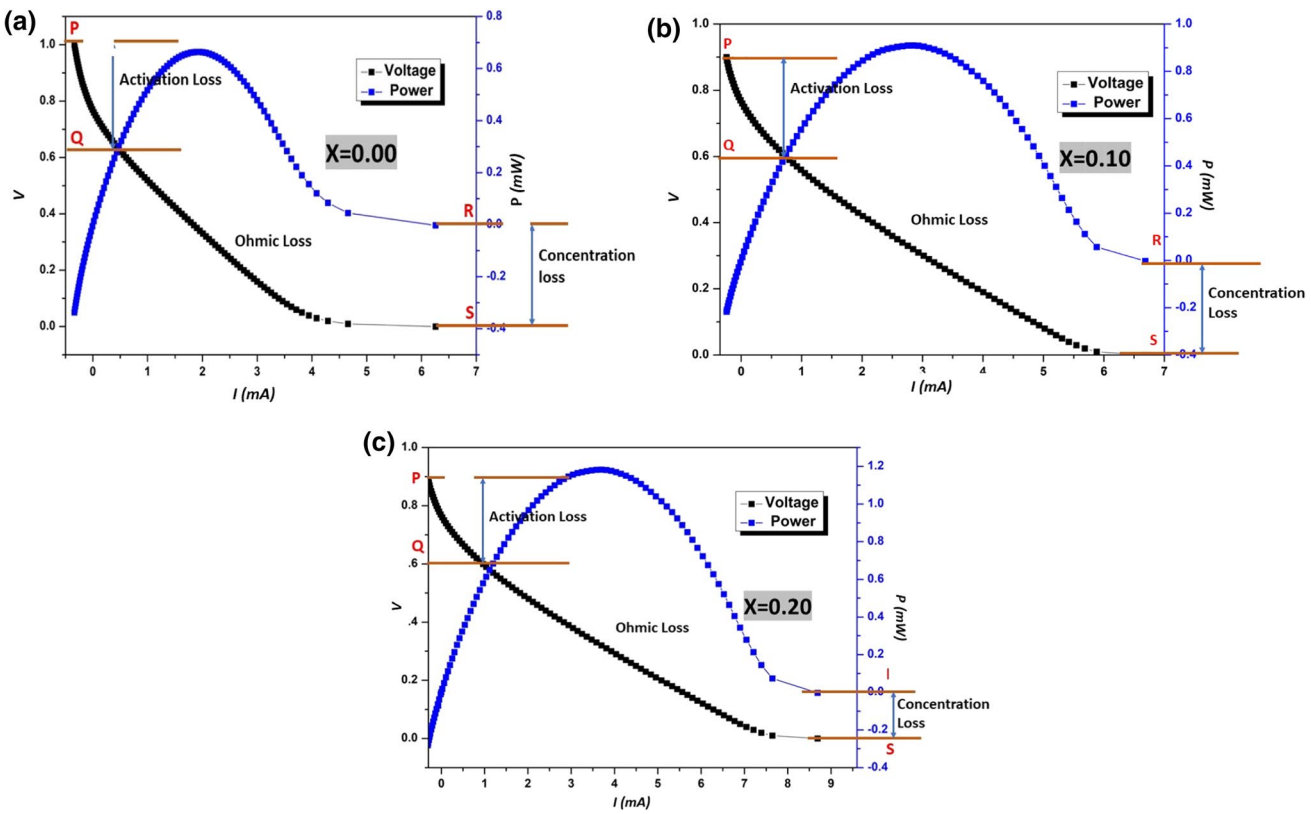

Fig. 9 *V–I* polarization plots for the yttrium-doped cobalt ferrites ($CoY_xFe_{2-x}O_4$), (a) $x = 0.00$, (b) $x = 0.10$, and (c) $x = 0.20$.

Table VIII Comparative study on the current values produced in the spinel ferrites based hydroelectric cells

Sample no.	Material used for fabricating HECs	Current (mA)	Synthesis method used	Area of the HECs (cm^2)	References
1.	$MgFe_2O_4$, $Ce_{0.1}MgFe_{1.9}O_4$	8.4	Co-precipitation	4.84	30
2.	$Mg_{0.8}Li_{0.2}Fe_2O_4$	8	Solid-state	4.84	8
3.	$Mg_{1-x}Na_xFe_2O_4$ ($x = 0.0, 0.1$)	1.2 and 7	Sol–gel	6.25	34
4.	$MgGd_{0.02}Fe_{1.98}O_4$	6.8	Sol–gel	4	35
5.	Al_2O_3, $Al_{1.9}Mg_{0.1}O_3$	4.5, 7	Solid-state reaction	4	36
6.	BTO-CFO	7.93	Sol–gel	4.5	37
7.	Red mud	7.6	Solid-state	6.25	38
8.	$NiFe_2O_4$	6.98	Solid-state reaction	20.25	39
9.	$Mg_{1-x}K_xFe_2O_4$, ($x = 0.00, 0.1, 0.2, 0.3$, and 0.4)	1.4-7.8	Sol–gel using citric acid	4	40
10.	$CoY_xFe_{2-x}O_4$, ($x = 0$, 0.10, and 0.20)	8.6	Sol–gel auto-combustion synthesis	4	Current work

of a HEC. Zn acts as the anode and behaves as a Lewis acid which can attract the lone pair electrons of oxygen of the H_2O molecule. Oxygen vacancies or the defects present on the surface of the ferrites trap electrons and act as donors, which attracts the positive side of the water molecules. As a result, the hydrogen bonding between the water molecules breaks down due to the electrostatic interaction between the oxygen vacancies and the positive ions of the water molecules.[33] Hence, the dissociation of polar H_2O molecules takes place on the surface of the HEC. This process is called chemi-dissociation and leads to the spreading of an OH^- layer over the surface of the ferrites. This chemisorbed OH^- layer further attracts the water molecules via hydrogen bonding, while the hopping of H^+ ions in the physisorbed layer takes place and gets caught inside the nanopores present in the ferrites. This trapping of H^+ ions creates enough electric potential to further dissociate the water molecules in the physisorbed water layers. OH^- ions migrate through the oxygen vacancies collected at the zinc anode leading to the oxidation of zinc to zinc hydroxide, releasing $2e^-$ to the Ag cathode where H_3O^+ ions are reduced to evolve H_2 gas. This redox electrochemical reaction at both the Zn and Ag electrodes leads to the generation of current and voltage in a HEC.

The possible electrochemical reaction involved in water dissociation are written as follows:

Dissociation of water molecule given by:

$$4H_2O \rightarrow 2H_3O^+ + 2OH^-, \tag{8}$$

Oxidation of OH^- at the Zn anode given by :

$$Zn \rightarrow Zn^{2+} + 2e^-$$

$$Zn^{2+} + 2OH^- \rightarrow Zn(OH)_2 \tag{9}$$

Reduction of hydronium ions at the Ag cathode given by:

$$2H_3O^+ + 2e^- \rightarrow H_2(\uparrow) + 2H_2O \tag{10}$$

Capacitive Behavior for Dry and Wet Hydroelectric Cells

The behavior of capacitance with respect to frequency for dry as well as wet HECs of yttrium-doped cobalt ferrites obtained at RT is shown in Fig. 10a, b, and c. A significant rise in the value of capacitance of Y^{3+} -doped cobalt ferrite HEC pellets has been observed with respect to pure cobalt ferrite HEC pellets. This is due to the creation of local dipoles with the rise in the content of Y^{3+} ions.[41] The dissociated ions (H_3O^+ and OH^-) on the surface of the HEC pellets as well as inside the lattice will create an interfacial charge region which is the possible reason behind the increased capacitance in the wet HECs. Thus, increased capacitance supports more chemi-dissociation of water molecules on the surface of the pellets.[42]

In the typical low-frequency range (20–100 Hz), the value of capacitance is high or the noise contribution is relatively high compared to the values in the higher-frequency range. In the low-frequency regime, the Maxwell–Wagner–Sillars effect becomes more effective.[40–42] This effect generally dominates in the heterogeneous systems or composites or doped ferrites. In ferrites, this effect rises due to the presence of grain boundaries or the interfaces present within the material. At low frequencies, charge carriers like ions or electrons have sufficient time to cross the grain boundaries which results in enhanced capacitive behavior or noisy data in the low-frequency range. The capacitance in wet form is relatively high compared to that in dry form. This behavior is mainly attributed due to the high dipole moment of polar water molecules, due to which they can align themselves in the direction of the applied field and contribute towards polarization. Also, the mobility of ions in the wet form is

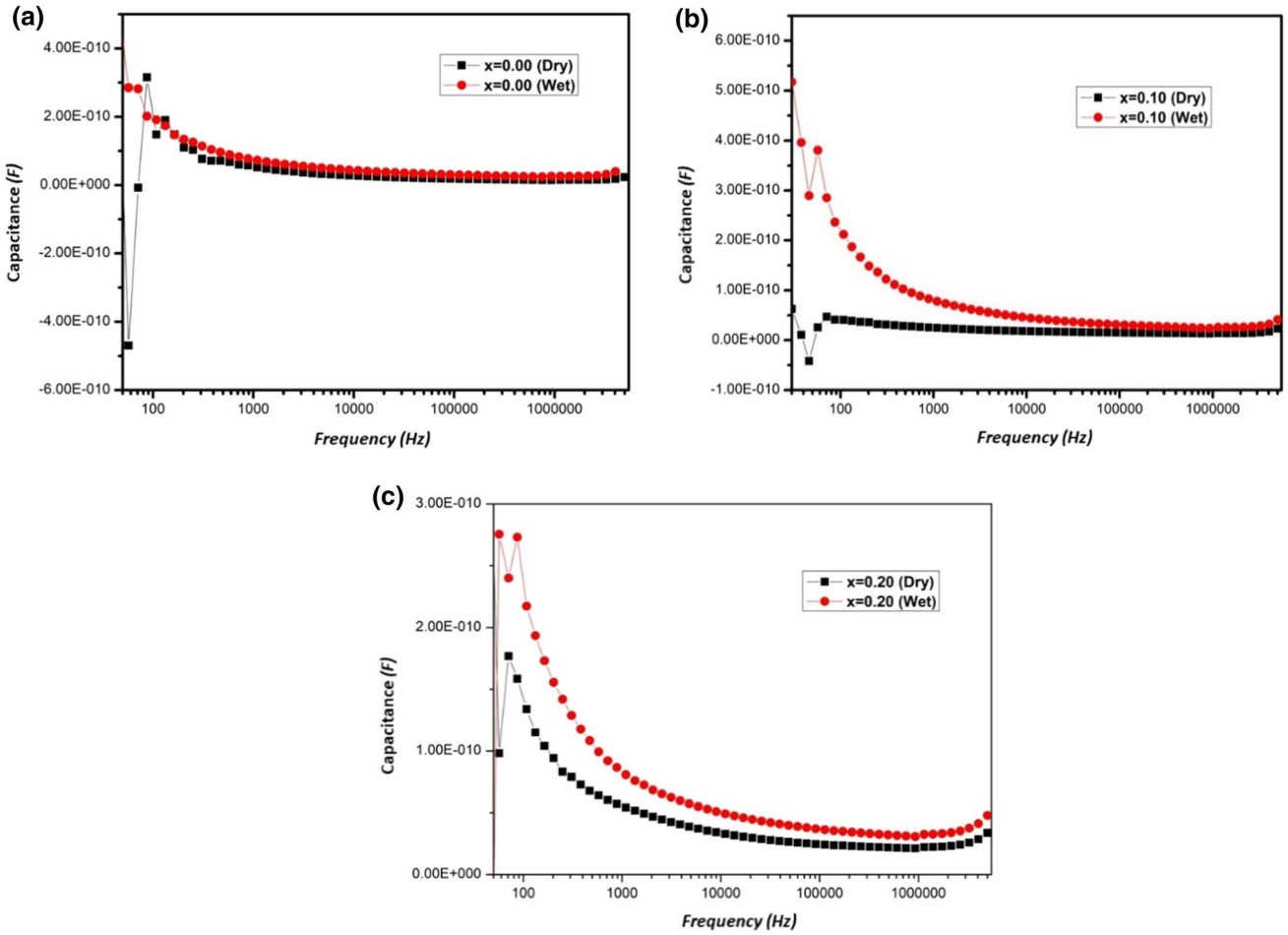

Fig. 10 Capacitance against frequency (50 Hz–1 MHz) for yttrium-doped cobalt ferrites ($CoY_xFe_{2-x}O_4$), (a) 0.00, (b) 0.10, and (c) 0.20.

more compared to the dry state due to which its capacitance has increased.

Impedance Spectroscopy for Dry and Wet Samples

Electrochemical impedance spectroscopy is a highly sensitive technique to analyze the mechanism of charge transfer or ionic diffusion mechanism in dry as well as wet HECs. Nyquist plots (Z'' versus Z') have been obtained for dry and wet hydroelectric cells at RT, as shown in Fig. 11a, b, and c. It has been observed that the dry HECs show very high values of impedance in the order of 10^6–10^7 ohms while wet HECs exhibit resistance in the order of 10^3–10^4 ohms. So, this reduction in the value of resistance for wet HECs confirms the adsorption of water molecules on the ferrite surface.[43] This shows that, by increasing the doping % of yttrium, an increase in the chemi-dissociation of water has taken place. The value of resistance (R_1) is found to be the minimum for the composition $x = 0.20$. Hence, the mechanism of transfer of ions towards the respective electrode is fast for the highest doping % of yttrium. Thus, the maximum current has been achieved by 20% yttrium-doped cobalt ferrite-based HECs.

Conclusions

Yttrium-doped cobalt ferrite ($CoY_xFe_{2-x}O_4$, $x = 0.00$, 0.10, 0.20) nanoparticles have been prepared using sol–gel auto-combustion synthesis. XRD measurements confirmed that the overall porosity (%) increased with increasing the yttrium content in the cobalt ferrites. FESEM showed spherical-shaped nanoparticles with the increase in homogeneity upon doping with yttrium. EDX ensured the presence of all the elements in the prepared material. Ferromagnetic studies revealed that the doping of yttrium in CFO can make stronger magnets which will be difficult to demagnetize due to the high value of coercivity. It has been concluded from *V–I* studies that the 10% yttrium-doped cobalt ferrite HECs exhibit very much less mass concentration loss and exhibit very much less value of resistance in its wet form. The fabricated HECs using 10% Y doped CFO showed the

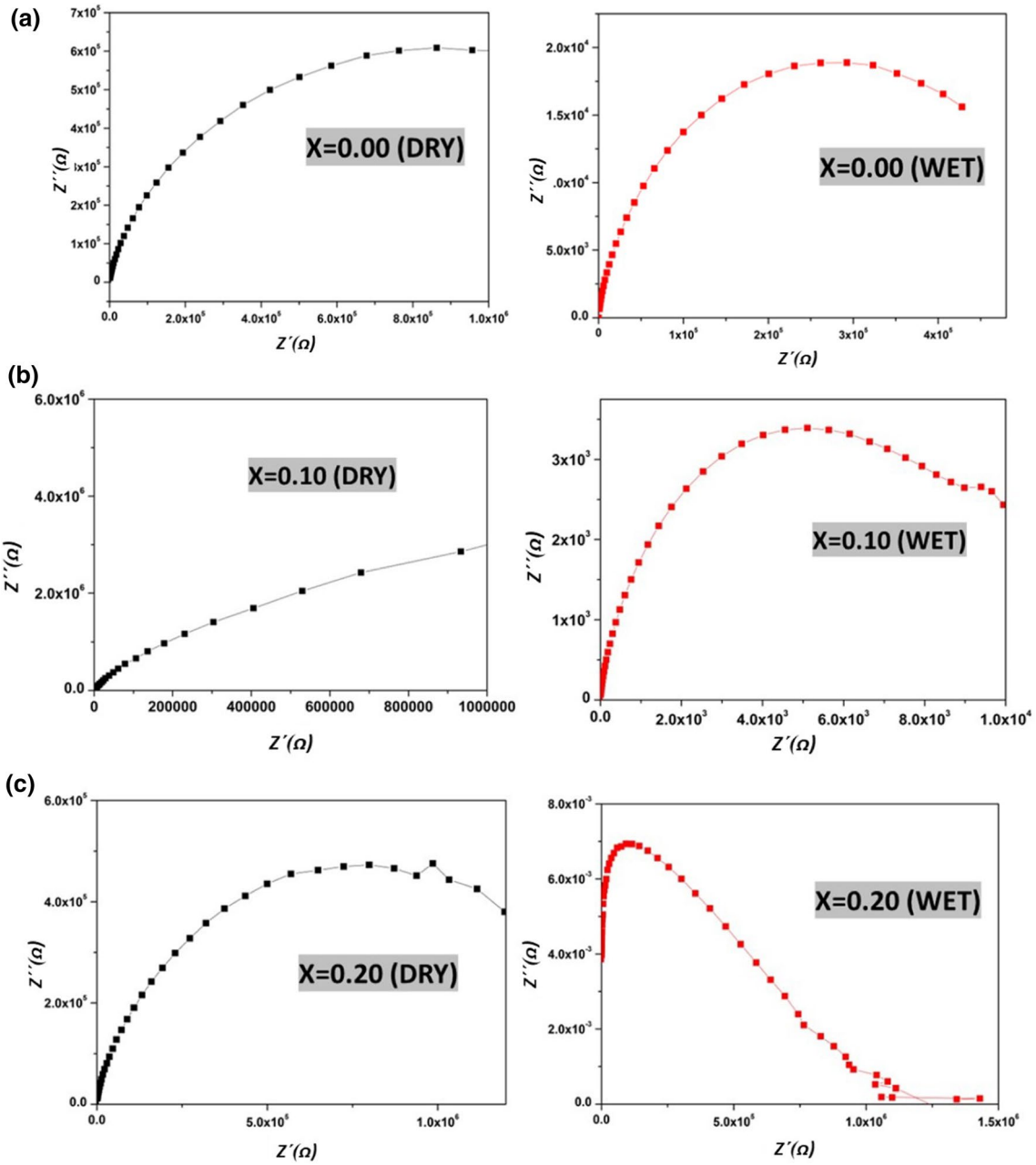

Fig. 11 Plot of voltage against current for the different compositions of yttrium-doped cobalt ferrites ($CoY_xFe_{2-x}O_4$) hydroelectric cells, (a) $x = 0.00$, (b) $x = 0.10$, (c) $x = 0.20$)

maximum output offload current of 8.3 mA, which is high compared to the current in pure cobalt ferrite ($I = 6.2$ mA). Thus, the *V–I* performance of the cobalt ferrites doped with yttrium-based HECs suggests its useful application in electricity generation.

Supplementary Information The online version contains supplementary material available at https://doi.org/10.1007/s11664-024-11178-7.

Acknowledgments Authors would like to thank USIC, Delhi University, for the XRD, FESEM, and magnetic measurements.

Conflict of interest The authors declare that they have no conflict of interest.

References

1. P. Jain, O.P. Thakur, and S. Shankar Subramanian, Structural, dielectric and impedance phenomena in copper ferrite nano powders for hydroelectric cell application. *Mater. Sci. Forum* 1099, 157–162 (2023).

2. P. Jain, S. Shankar, and O.P. Thakur, Structural, dielectric, impedance, ferroelectric studies of zinc doped bismuth ferrites for hydroelectric cell application, in *International Conference on Sustainable Technologies and Advances in Automation, Aerospace and Robotics* (2022), pp. 505–513.
3. I.H. Gul and A. Maqsood, Structural, magnetic and electrical properties of cobalt ferrites prepared by the sol–gel route. *J. Alloys Compd.* 465(1–2), 227–231 (2008).
4. C. Murugesan and G.J.R.A. Chandrasekaran, Impact of Gd^{3+} substitution on the structural, magnetic and electrical properties of cobalt ferrite nanoparticles. *RSC Adv.* 5(90), 73714–73725 (2015).
5. L. Avazpour, H. Shokrollahi, M.R. Toroghinejad, and M.A. Zandi Khajeh, Effect of rare earth substitution on magnetic and structural properties of $Co_{1-x}RE_x$ Fe_2O_4 (RE: Nd, Eu) nanoparticles prepared via EDTA/EG assisted sol–gel synthesis. *J. Alloys Compd.* 662, 441–447 (2016).
6. S. Amiri and H. Shokrollahi, Magnetic and structural properties of RE doped Co-ferrite (REåNd, Eu, and Gd) nano-particles synthesized by co-precipitation. *J. Magn. Magn. Mater.* 345, 18–23 (2013).
7. F. Cheng, C. Liao, J. Kuang, Z. Xu, C. Yan, L. Chen, H. Zhao, and Z. Liu, Nanostructure magneto-optical thin films of rare earth (RE= Gd, Tb, Dy) doped cobalt spinel by sol–gel synthesis. *J. Appl. Phys.* 85(5), 2782–2786 (1999).
8. R.K. Kotnala and J. Jyoti Shah, Green hydroelectrical energy source based on water dissociation by nanoporous ferrite. *Int. J. Energy Res.* 40(12), 1652–1661 (2016).
9. J. Shah, R. Gupta, and R.K. Kotnala, Colossal humidoresistance inducement in magnesium ferrite thin film led to green energy device invention: hydroelectric cell, in *Recent Advances in Thin Films* (2020), pp. 389–411.
10. R.K. Kotnala, R. Gupta, A. Shukla, S. Jain, A. Gaur, and J. Shah, Metal oxide based hydroelectric cell for electricity generation by water molecule dissociation without electrolyte/acid. *J. Phys. Chem. C* 122(33), 18841–18849 (2018).
11. S. Jain, J. Shah, N.S. Negi, C. Sharma, and R.K. Kotnala, Significance of interface barrier at electrode of hematite hydroelectric cell for generating ecopower by water splitting. *Int. J. Energy Res.* 43(9), 4743–4755 (2019).
12. S. Saini, J. Shah, R.K. Kotnala, and K.L. Yadav, Nickel substituted oxygen deficient nanoporous lithium ferrite based green energy device hydroelectric cell. *J. Alloys Compd.* 827, 154334 (2020).
13. P. Jain, S. Subramanian, and O.P. Thakur, Advancements in multiferroic, dielectric, and impedance properties of copper-yttrium Co-doped cobalt ferrite for hydroelectric cell applications. *J. Phys. Condens. Matter* 36, 295201 (2024).
14. D.T. Rahardjo, S. Budiawanti, S. Suharno, R. Suryana, A. Supriyanto, and B. Purnama, Effect of yttrium-doping on structural and magnetic properties in cobalt ferrite nanoparticles prepared by the sol–gel auto-combustion procedure, in *AIP Conference Proceedings*, vol. 2604, no. 1 (AIP Publishing, 2023).
15. A. Joshi, R.C. Srivastava, R. Dhyani, and C.S. Joshi, Structural, magnetic, and dielectric properties of yttrium-doped cobalt ferrite and their nanocomposites with polythiophene. *J. Magn. Magn. Mater.* 578, 170812 (2023).
16. V.R. Bhagwat, A.V. Humbe, S.D. More, and K.M. Jadhav, Sol–gel auto-combustion synthesis and characterizations of cobalt ferrite nanoparticles: different fuels approach. *Mater. Sci. Eng. B* 248, 114388 (2019).
17. D. Narsimulu, O. Padmaraj, E.S. Srinadhu, and N. Satyanarayana, Synthesis, characterization and electrical properties of mesoporous nanocrystalline $CoFe_2O_4$ as a negative electrode material for lithium battery applications. *J. Mater. Sci. Mater. Electron.* 28, 17208–17214 (2017).
18. M.F. Zawrah, M.M. El-Okr, A. Ashery, and A.B. Abou Hammad, Characterization of sol–gel fabricated cobalt ferrite $CoFe_2O_4$ nanoparticles. *Middle East J. Appl. Sci.* 6, 362–366 (2016).
19. M. Mostafa, O. Saleh, A.M. Henaish, S.A.A. El-Kaream, R. Ghazy, O.M. Hemeda, A.M. Dorgham, H. Al-Ghamdi, A.H. Almuqrin, M.I. Sayyed, S.V. Trukhanov, E.L. Trukhanova, A.V. Trukhanov, D. Zhou, and M.A. Darwish, Structure, morphology and electrical/magnetic properties of Ni-Mg nano-ferrites from a new perspective. *Nanomaterials* 12(7), 1045 (2022).
20. T.E.P. Alves, H.V.S. Pessoni, and A. Franco Jr., The effect of Y^{3+} substitution on the structural, optical band-gap, and magnetic properties of cobalt ferrite nanoparticles. *Phys. Chem. Chem. Phys.* 19(25), 16395–16405 (2017).
21. S.B. Das, R.K. Singh, V. Kumar, N. Kumar, P. Singh, and N.K. Naik, Structural, magnetic, optical and ferroelectric properties of Y^{3+} substituted cobalt ferrite nanomaterials prepared by a cost-effective sol–gel route. *Mater. Sci. Semicond. Process.* 145, 106632 (2022).
22. S. Kumari, V. Kumar, P. Kumar, M. Kar, and L. Kumar, Structural and magnetic properties of nanocrystalline yttrium substituted cobalt ferrite synthesized by the citrate precursor technique. *Adv. Powder Technol.* 26(1), 213–223 (2015).
23. A. Kiran, M.N. Akhtar, M. Yousaf, K.M. Batoo, O.M. Aldossary, and S.N. Khan, Influence of Y^{3+}, Yb^{3+}, Gd^{3+} cations on structural and electromagnetic properties of $CuFe_2O_4$ nanoferrites prepared via one step sol–gel method. *J. Rare Earths* 39(10), 1224–1231 (2021).
24. F.R. Mariosi, J. Venturini, A. da Cas Viegas, and C.P. Bergmann, Lanthanum-doped spinel cobalt ferrite ($CoFe_2O_4$) nanoparticles for environmental applications. *Ceram. Int.* 46(3), 2772–2779 (2020).
25. S. Chakrabarty, A. Dutta, and M. Pal, Effect of yttrium-doping on structure, magnetic and electrical properties of nanocrystalline cobalt ferrite. *J. Magn. Magn. Mater.* 461, 69–75 (2018).
26. M.A. Abdo, S.F. Mansour, N.S. Al-Bassami, and N.I. Abu-Elsaad, Yttrium substituted Co–Cu–Zn nanoferrite: a synergetic impact of Y^{3+} on enhanced physical properties and photocatalysis. *Ceram. Int.* 48(11), 15314–15326 (2022).
27. C.N. Chinnasamy, M. Senoue, B. Jeyadevan, O. Perales-Perez, K. Shinoda, and K.T. Chinnasamy, Synthesis of size-controlled cobalt ferrite particles with high coercivity and squareness ratio. *J. Colloid Interface Sci.* 263(1), 80–83 (2003).
28. H. Hemanta Singh, E. Churchill Singh, and H. Basantakumar Sharma, Synthesis of yttrium and cobalt doped bismuth ferrite nanoparticles for electrical and magnetic properties. *Integr. Ferroelectr.* 203(1), 108–119 (2019).
29. M.M. Rhaman, M.A. Matin, M.N. Hossain, M.N.I. Khan, M.A. Hakim, and M.F. Islam, Ferromagnetic, electric, and ferroelectric properties of samarium and cobalt Co-doped bismuth ferrite nanoparticles. *J. Phys. Chem. Solids* 147, 109607 (2020).
30. I.A. Parray, A. Somvanshi, and S.A. Ali, Study of microstructural, ferroelectric and magnetic properties of cerium substituted magnesium ferrite and its potential application as hydroelectric cell. *Ceram. Int.* 49(4), 6946–6957 (2023).
31. R.K. Singh, D. Rangappa, N. Kumar, J. Shah, V. Kumar, and R.K. Kotnala, Tailoring the physical properties of non-molar potassium-substituted magnesium ferrite nanomaterials and its applications in hydroelectric cell. *Appl. Phys. A* 129(1), 15 (2023).
32. R.K. Kotnala, S. Saini, J. Shah, and K.L. Yadav, Significant role of defect-induced surface energy in water splitting to generate electricity by nickel ferrite hydroelectric cell. *Int. J. Energy Res.* 46(5), 6421–6435 (2022).
33. P. Jain, S. Shankar, and O.P. Thakur, Unveiling the impact of Ni^{2+}/Y^{3+} co-substitution on the structural, dielectric, and impedance properties of multiferroic spinel ferrite for hydroelectric

cell application. *Phys. Chem. Chem. Phys.* 25(32), 21280–21296 (2023).
34. V. Kumar, R.K. Singh, A. Manash, S.B. Das, J. Shah, and R.K. Kotnala, Structural, optical and electrical behaviour of sodium-substituted magnesium nanoferrite for hydroelectric cell applications. *Appl. Nanosci.* 13(6), 4573–4591 (2023).
35. I.A. Parray, S.A. Ali, R. Khan, J. Shah, and R.K. Kotnala, Green energy generation via water splitting by non-photocatalytic process based on Gd doped magnesium ferrite hydroelectric cell. Available at SSRN 4623639.
36. R. Gupta, J. Shah, R. Das, S. Saini, and R.K. Kotnala, Defect-mediated ionic hopping and green electricity generation in $Al_{2-x}Mg_xO_3$-based hydroelectric cell. *J. Mater. Sci.* 56, 1600–1611 (2021).
37. J. Shah, K.C. Verma, A. Agarwal, and R.K. Kotnala, Novel application of multiferroic compound for green electricity generation fabricated as hydroelectric cell. *Mater. Chem. Phys.* 239, 122068 (2020).
38. R.K. Kotnala, R. Das, J. Shah, S. Sharma, C. Sharma, and P.B. Sharma, Red mud industrial waste translated into green electricity production by innovating an ingenious process based on hydroelectric cell. *J. Environ. Chem. Eng.* 10(2), 107299 (2022).
39. P. Kumar, P. Kumar, M.K. Kansal, V. Bhardwaj, and V. Verma, Green energy production by $NiFe_2O_4$ based hydroelectric cells. *Mater. Today Proc.* (2023). https://doi.org/10.1016/j.matpr.2023.04.263.
40. A. Manash, R.K. Singh, V. Kumar, S.B. Das, S.S. Kumar, N. Kumar, J. Shah, and R.K. Kotnala, Studies on structural and optical behavior of nanoporous potassium-substituted magnesium ferrite nanomaterials, and their application as a hydroelectric cell. *J. Mater. Sci. Mater. Electron.* 33(28), 22103–22118 (2022).
41. R. Gupta, J. Shah, R. Singh, and R.K. Kotnala, Nonphotocatalytic water splitting process to generate green electricity in alkali doped zinc oxide based hydroelectric cell. *Energy Fuels* 35(11), 9714–9726 (2021).
42. M.A. Rahman and A.K.M. Akther Hossain, Relaxation mechanism of $(x)Mn_{0.45}Ni_{0.05}Zn_{0.50}Fe_2O_4+(1-x)BaZr_{0.52}Ti_{0.48}O_3$ multiferroic materials. *Phys. Scr.* 89(11), 115811 (2014).
43. P. Jain, S. Shankar, and O.P. Thakur, Exploring the multiferroic and water sensing behavior of Cu/Er Co-substituted ferrites as key enablers for next-gen hydroelectric cells. *Mater. Chem. Phys.* 315, 128945 (2024).